



## Pacific trench motions controlled by the asymmetric plate configuration

Thorsten J. Nagel,<sup>1</sup> William B. F. Ryan,<sup>2</sup> Alberto Malinverno,<sup>2</sup> and W. Roger Buck<sup>2</sup>

Received 6 July 2007; revised 8 January 2008; accepted 29 February 2008; published 23 May 2008.

[1] We present a novel explanation for absolute trench-normal motions of slabs surrounding the Pacific. Rapid subduction-zone retreat on the eastern side of the Pacific and slow advance in the west can result from the large-scale asymmetric plate configuration. We use simple fluid dynamics to explain the mechanical background of this hypothesis, and we use the results of a simple finite difference scheme to estimate the effect on trench motion velocities. The hypothesis is based on two key assumptions. First, we follow the concept of plate-scale horizontal counterflow in the asthenosphere driven by accretion of asthenosphere into lithosphere and by plate motion. Second, we assume that horizontally wide slabs without large slab windows drift passively in the mantle flow field and do not retreat as a result of flow around the slab. If the asthenosphere transfers flow-related horizontal shear stress into deeper levels of the mantle, an asymmetry in the plate configuration leads to different net pressure forces on the two slabs and thus affects the retreat behavior. In an ocean with an asymmetric ridge position, the slab of the smaller plate should retreat faster than the slab of the large plate, which may even advance. Also, the domain of a slower moving plate should collapse faster than the domain of the faster plate. Our model explains the counterintuitive negative correlation between slab age and retreat velocity observed in the Pacific. It also accords with the topographic asymmetry of the ridge flanks along the Pacific rise. **Citation:** Nagel, T. J., W. B. F. Ryan, A. Malinverno, and W. R. Buck (2008), Pacific trench motions controlled by the asymmetric plate configuration, *Tectonics*, 27, TC3005, doi:10.1029/2007TC002183.

### 1. Absolute Trench Motion

[2] In 1978, Clement Chase published a groundbreaking map which displayed absolute motions of upper and lower plates along the convergent plate boundaries surrounding the

Pacific. The map showed all lower plates and almost all upper plates moving in the direction of the trenches [Chase, 1978]. Those upper plates that moved away from the trench, such as the Australian Plate at the Tonga Trench or the Philippine Plate at the Mariana Trench, showed active back-arc spreading and Chase assumed that this extension balanced the upper plate motion away from the trench. He inferred that all slabs probably retreat, or at least are stationary in the hot spot reference frame, and viewed his observations as a strong argument for slab pull being the imperative plate-driving force [Moberly, 1972; Forsyth and Uyeda, 1975; Molnar and Atwater, 1978; Uyeda and Kanamori, 1979]. Ever since, the mechanics of slab retreat have been a major subject of tectonic research. The concept of slabs sinking into the mantle more or less vertically, i.e., with a motion vector steeper than the dip of the slab, explained the existence of several subduction-back-arc systems without significant plate convergence such as the Mediterranean subduction zones [e.g., Malinverno and Ryan, 1986; Gautier et al., 1999; Faccenna et al., 2001; Faccenna et al., 2004]. In the past years, studies on the dynamics of trench-normal slab motions have been fuelled by advanced physical models, the possibility to image ductile deformation in the upper mantle through seismic data, and the advent of cheap powerful computers allowing for two- and three-dimensional numerical modeling of subduction processes [Rizzetto et al., 2004; Funicello et al., 2004; Gurnis et al., 2004; Enns et al., 2005; Pysklywec and Ishii, 2005; Funicello et al., 2006; Stegman et al., 2006; Schellart et al., 2007]. Slab retreat is often viewed as resulting from slab pull overpressuring the viscous mantle beneath the subducting plate and thus driving flow around the slab into the domain of the overriding plate. Several recent studies have focused on this kind of upper mantle flow from one side of the slab toward the other and how the local framework, for example, the existence or absence of slab windows, the width and/or depth of a slab, or the physical properties of the slab, controls retreat velocity. [e.g., Gurnis et al., 2004; Funicello et al., 2004; Bellahsen et al., 2005; Funicello et al., 2006; Stegman et al., 2006; Piromallo et al., 2006; Royden and Husson, 2006; Schellart et al., 2007; Faccenna et al., 2007].

[3] Figure 1 shows a new version of Chase's map based on recent data for plate motions [Bird, 2003] in the HS3 reference frame [Gripp and Gordon, 2002]. Bird's plate model utilizes data from arcs and back arcs and defines several small arc plates. It also introduces a series of plate boundaries which account for deformation in eastern Asia and the American continents close to the subduction zones. Hence, upper plate motions in Figure 1 display trench motions corrected for back-arc deformation (neglecting

<sup>1</sup>Steinmar Institut, Universität Bonn, Bonn, Germany.

<sup>2</sup>Lamont-Doherty Earth Observatory of Columbia University, Palisades, New York, USA.

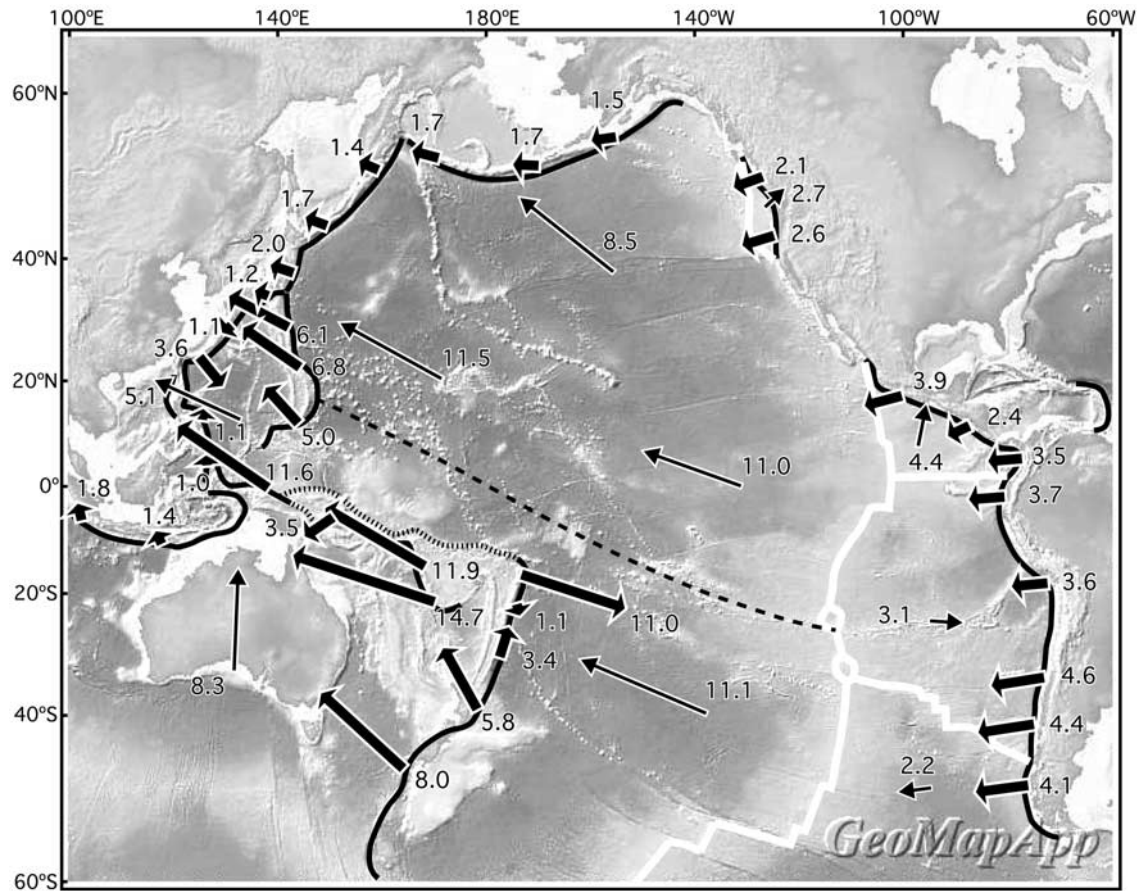


**Figure 1.** Map of the Pacific showing absolute motions of oceanic plates (thin arrows) and upper plates directly at the trench (thick arrows) which are considered as slab motions [Bird, 2003; Gripp and Gordon, 2002]. Dotted line indicates equator of the Pacific plate motion.

accretion and erosion at the plate boundary). A picture significantly different from Chase's map emerges. Slabs in the eastern Pacific with the American continents as over-riding plates retreat at rates between 2 and 4.5 cm/a. However, subduction zones in the northwestern Pacific beneath the Asian continental lithosphere, i.e., the Kuril and Japan trenches, advance toward Asia with velocities up to 2 cm/a. Slabs on the western side of the Philippine plate are about stationary or advance very slowly ( $\leq 1$  cm/a) except for the southern Ryukyu trench which retreats with velocities reaching 3 cm/a at the southern tip of the trench. The oceanic slab of the Australian plate, subducted along the Sunda trench also advances slowly toward Asia. Intraoceanic slabs in the Pacific display the highest velocities and advance (Mariana-Izu: 6 cm/a) or retreat (Tonga: 11 cm/a, Vanuatu: 14 cm/a). The Tonga and Vanuatu slabs also show remarkable variations along strike with retreat velocities increasing toward the tips of the slabs.

[4] In summary, trenches bordering the continents around the Pacific show fast rollback along the eastern side but slow advance or no motion in the west. Hence, the behavior of Pacific subduction zones is in conflict with two widely acknowledged notions: first, the association of absolute slab

retreat and back-arc extension and, second, the concept that old, heavy lithosphere would be prone to rollback [Molnar and Atwater, 1978].

[5] Absolute motions in Figure 1, which are calculated from published models [Bird, 2003; Gripp and Gordon, 2002] confirm findings of Heuret and Lallemand [2005] and Lallemand *et al.* [2005]. These authors performed a statistical study on global absolute trench motions using the same HS3 reference frame and geodetic data for back-arc deformation. They identified the same advancing and retreating slabs and a startling negative correlation between slab age and retreat velocity (Figure 2). Slabs of old lithosphere advance, slabs of young lithosphere retreat [Faccenna *et al.*, 2007]. Heuret and Lallemand [2005] concluded that lateral slab motions must to a large extent be controlled by plate-scale mantle flow rather than by the gravitational instability of the slab. Recently, Faccenna *et al.* [2007] explained the observed age-retreat relationship through plate properties. Older plates would be thicker and thus harder to bend in the trench corner. Hence, thin and young plates would retreat easily whereas bending of thicker plates would require an additional mantle drag through slab advance.

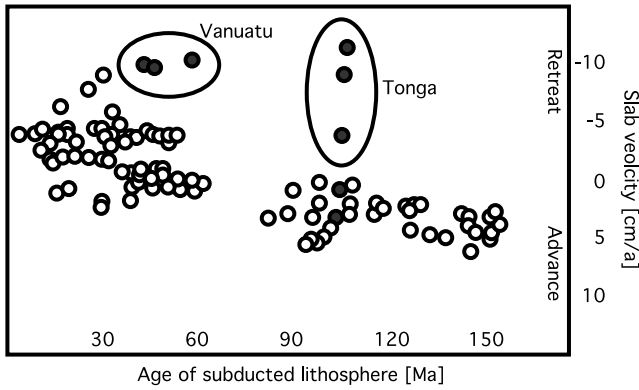


**Figure 2.** Relationship between slab age and absolute retreat velocity of trenches in the Pacific [from Heuret and Lallemand, 2005]. Filled dots mark Vanuatu and Tonga slabs. Extremely high retreat velocities along the Tonga trench are from the northern end of the slab (Figure 1).

[6] Obviously, absolute velocities displayed in Figures 1 and 2 depend on the chosen reference frame HS3. Of all common reference frames, HS3 has the largest net rotation, i.e., westdrift of the lithosphere [e.g., Enns et al., 2005; Becker, 2006]. Using other reference frames like SB04 [Steinberger et al., 2004] or a No-Net-Rotation frame [DeMets et al., 1994; Gripp and Gordon, 2002] would obliterate or even reverse the trend in Figure 2 since the No-Net-Rotation frame basically fixes the South American trenches. The HS3 reference frame, however, is the only one to include Pacific hot spots. Hence, to the extent that Pacific hot spots constrain the motion of Pacific trenches relative to the deeper mantle we need an explanation for the observed negative correlation of plate age and retreat rate.

## 2. Asymmetric Plate Architecture and Regional Mantle Flow

[7] Here, we assume that wide slabs around the Pacific represent impermeable barriers separating the asthenosphere

of the upper and lower plate. Slabs would thus sail passively in the subplate mantle flow and this flow would be imaged by absolute trench motions. We present a hypothesis how a flow pattern consistent with slow trench advance in the west and rapid trench retreat in the east can result from the asymmetric plate configuration. The hypothesis is based on a classic model about the nature of the sublithospheric mantle [Morgan, 1971; Schubert and Turcotte, 1972; Schubert et al., 1976] (Figure 3). Beneath the oceanic plates, a layer of low density and viscosity (asthenosphere) rests on top of denser and more viscous mantle (mesosphere) and this stratification is relatively stable, i.e., defined by the composition, the water content [e.g., Richards et al., 2001] or thermal properties of the two. The flow pattern in the asthenosphere is controlled by plate motion and by accretion of asthenosphere into lithosphere [Chase, 1979; Parmentier and Oliver, 1979; Morgan and Smith, 1992; Morgan et al., 1995]. Diverging plates drag asthenosphere away from the mid-ocean ridge toward the slab corners. Also, accretion takes place dominantly in the vicinity of divergent plate boundaries, where plate thickening rates are highest. The resulting deflation beneath the ridges and inflation in the trench corners create a pressure gradient driving return flow back to the ridge (Figure 3). Hence, gradients from low to high pressure beneath the oceanic lithosphere are oriented away from the ridge. This concept successfully explains a range of data sets, such as the topography of the abyssal plains [Morgan and Smith, 1992] and variations of topography and geochemical signature along the strike of ridges [e.g., Morgan et al., 1995; Small and Danyushevsky, 2003]. A vertically resisting lower boundary of viscous subplate mantle supporting horizontal pressure gradients has been used in many recent experimental studies on absolute trench motions, physical and numerical [e.g., Funiello et al., 2004; Funiello et al., 2006; Piromallo et al., 2006; Stegman et al., 2006; Schellart et al., 2007].

[8] We explore the effects of accretion and plate motion in an oceanic domain which consists of two subducting plates separated by a mid-ocean ridge (Figure 3). Asthenosphere gets accreted into the oceanic lithosphere and is subsequently subducted into the deeper mantle. If the

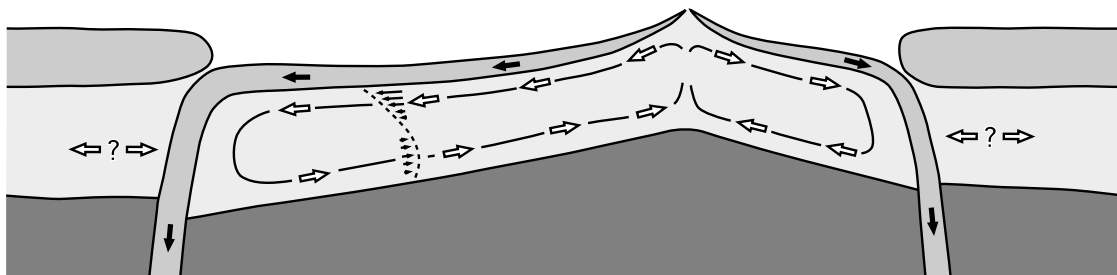


**Figure 3.** Cartoon illustrating the mechanical concept of counterflow in the asthenosphere [e.g., Turcotte and Schubert, 1982; Morgan et al., 1995]. Dominantly horizontal flow in the asthenosphere is caused by a density contrast at the base. Plate drag and accretion create a deflation at the ridge which pulls up the lower boundary to the high-density substratum and thus drives counterflow back to the ridge. We further assume that the lithosphere is subducted into the deeper mantle. This outflux from the asthenosphere leads to a continuous pressure drop in the oceanic domain and associated flow from the outside world toward the ocean. This flow causes slabs to retreat and the oceans to shrink.

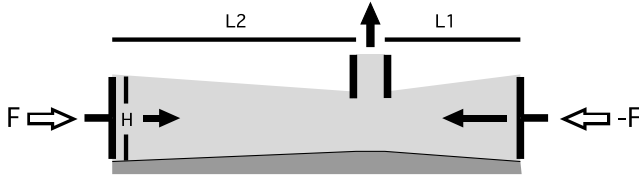


**Figure 4.** Model illustrating the effect of an asymmetric ridge location on the accretion-related component of flow in Figure 3. A domain of light fluid floats on a heavy fluid and is enclosed between two pistons. Each piston exerts a certain force  $F$  on the domain and this force is balanced by the pressure force of a fluid column with the height  $H$ . If the fluid is sapped at a position with a distance  $L_1$  to one of the pistons and  $L_2$  to the other with  $L_1 < L_2$  (corresponding to an asymmetric ridge location) the closer piston will move in faster. This happens as the topographic gradient driving collapse toward the drain is steeper on the shorter side. Hence, the slab of the shorter plate in Figure 3 would retreat faster as a result of asymmetric accretion.

asthenospheric reservoir is not refilled, this outflux will cause a continuous pressure drop and flow of viscous mantle from the outside world toward the oceanic domain. Slabs will retreat and the ocean will shrink. For a symmetric situation, i.e., with a nonmoving ridge in the center of the ocean, retreat velocities on both sides will be the same. However, in an asymmetric ocean the inside corners of the two slabs might exert different pressure forces toward the outside world and retreat velocities might differ. In the following, we discuss the consequences of asymmetric accretion and of asymmetric counterflow using basic fluid dynamic assumptions, i.e., the shallow-water approximation. These two processes are then combined in a simple finite difference scheme.

[9] The effect of an asymmetric ridge location on the accretion-related component of flow in the asthenosphere is relatively simple. Let us assume that the outside world exerts the same lithostatic pressure on the two slabs, causing retreat while the asthenospheric reservoir of the ocean is emptied. Since the pressure minimum in the oceanic asthenosphere is located at the ridge, where the asthenosphere is tapped, the pressure gradient beneath the larger plate has to be smaller than beneath the shorter plate and the shorter plate will collapse faster. As a model we consider a highly viscous, light fluid contained between two pistons and resting on a higher-density fluid (Figure 4). The pistons apply a force on the fluid which is balanced by the pressure force of the inside fluid columns. If the light fluid is sapped at a certain position, topographic tapers will develop on both sides (Figure 4). The associated pressure gradient will drive fluid toward the drain, the fluid level will drop, and the pistons will move inward. An asymmetric draining position will cause a steeper topographic gradient on the short side of the contained fluid. Hence, the short fluid wedge will drain more rapidly and the piston on that side will move in faster. If the flow-related difference of fluid height is small compared to the total fluid height  $H$ , the

retreat velocities  $v_1$  and  $v_2$  scale linearly with the pressure gradient so that

$$\frac{v_1}{L_2} = \frac{v_2}{L_1}, \quad (1)$$

with  $L_1$  and  $L_2$  being the lengths of the two sides. This mechanism alone could explain slower retreat of the larger plate's slab but not slab advance.

[10] The effect of an asymmetric ridge location on flow excited by plate motion is slightly more complicated. As a model, we imagine a wide layer of light fluid which is bounded by a rigid wall on the right side and floats on top of a heavy fluid. A thin belt envelops a portion of the fluid in the way shown in Figure 5. The belt can penetrate the wall but the fluid cannot and thus, a fixed amount of light fluid is trapped inside the belt. If no forces are applied to the belt, the fluid columns inside and outside the belt will naturally have the same height (Figure 5). Now, a downward load is put on the lower end of the belt (a slab pull force). In a first step, we consider a static case, in which the right end of the belt is attached to a vertically free bolt at the wall (Figure 6). The load force  $F_{pu}$  is transmitted along the belt around the contained fluid and finally pulls at the bolt in a horizontal direction (Figure 6a). The loaded belt pressurizes the inside fluid leading to thickening and shortening of the layer. The inside overpressure balancing the tension of the belt is provided by the excess elevation  $\Delta H$  of the inside fluid column, thus  $\rho g \Delta H$ . The precise shape of the belt can be calculated in the same way the size and pressure inside a soap bubble can be derived from the surface tension of the soap-air interface. The local curvature of the belt depends on the transmitted force and the local pressure difference between the inside and outside world. Along the portion of

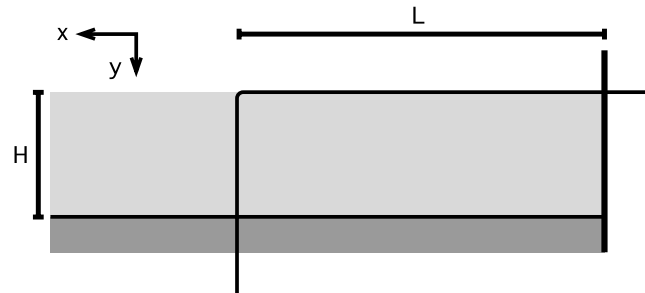


**Figure 5.** Model setup used to consider the effect of plate-motion-related counterflow on slab motion. A wide viscous layer of thickness  $H$  is floating on a heavy fluid and bounded on the right side by a fixed wall. A conveyor belt is free to penetrate through the wall and contains a certain amount of fluid. The location of the slab, i.e., the section of the belt crossing the fluid layer, depends on the forces exerted on the belt. With no forces besides pressure forces of the fluid, the fluid columns inside and outside the belt have the same height, which determines the horizontal length of the belt  $L$ . Small arrows indicate positive  $x$  and  $y$  directions in equations derived in the text.

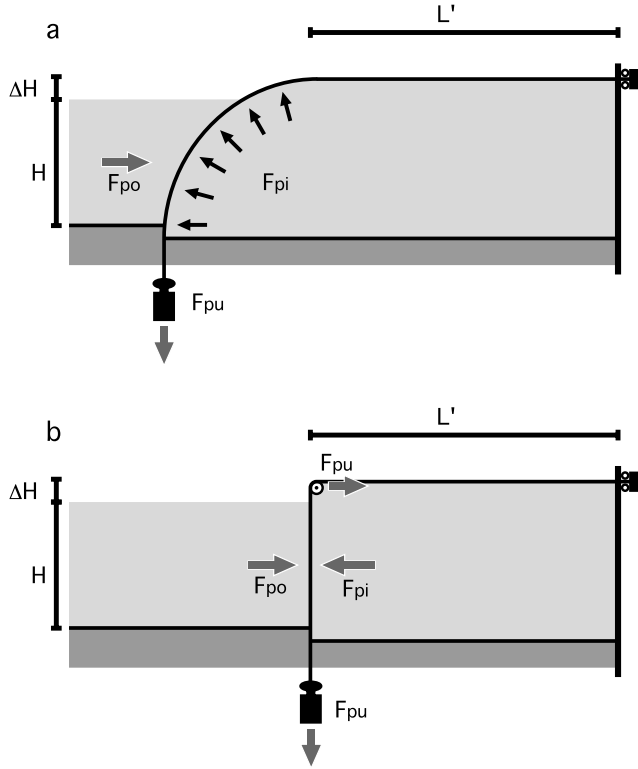


**Figure 6.** The right side of the belt in Figure 5 is attached to a vertically free-moving bolt at the wall and a pull force is applied at the other end.  $F_{pu}$ , pull force at the belt;  $F_{pi}$ , inside pressure force on the belt;  $F_{po}$ , outside pressure force on the belt. (a) The pull force  $F_{pu}$  is transmitted along the belt and the slab assumes a circular shape inside the fluid layer. The tension of the belt pressurizes the inside fluid and causes thickening of the fluid layer, i.e., a rightward dislocation of the slab as compared to Figure 5. The equilibrium thickness of the slab (with an inside layer length  $L'$ ) is defined by an extra elevation of the fluid column  $\Delta H$  that creates an extra pressure force on the vertical projection of the slab balancing the pull force  $F_{pu}$ . (b) For  $L' \gg H$  and  $H \gg \Delta H$ , the model in Figure 6a can be considered as having a belt with a horizontal section and a vertical slab separated by a pivot.  $\Delta H$  is same as in Figure 6a and defined by the horizontal extra pressure force  $\Delta H \rho g H$  balancing the pull force  $F_{pu}$  transmitted along the belt.

the belt inside the fluid, i.e., the slab, the pressure difference is constant causing a circular shape of the belt (Figure 6a). In any direction, the load force  $F_{pu}$  transmitted along the belt (the “surface tension” of the belt) has to be equal to the excess pressure force applied in the opposite direction on the projection of the belt perpendicular to that direction. For variations in layer thickness being small compared to the total thickness of the layer, the excess pressure force in the horizontal direction would be the excess pressure  $\rho g \Delta H$  applied on the vertical projection of the belt, which is simply the layer thickness  $H$ . We can thus write

$$\Delta H \rho g H = -F_{pu}, \quad (2)$$

with  $F_{pu}$  being the pull force per meter parallel to the trench,  $H$  being the thickness of the fluid layer,  $\Delta H$  the excess elevation of the fluid column inside the belt,  $\rho$  the density of the fluid,  $g$  the gravitational acceleration, and  $F_{pu}$  the load at the belt. If the layer thickness  $H$  is small compared to the horizontal length  $L'$  of the inside fluid, the area beneath the curved portion of the belt in the trench corner can be neglected. For future calculations we assume that the belt runs over a pivot and crosses the fluid layer vertically (Figure 6b). The force balance remains the same as in equation (2). An equilibrium situation is reached when the excess inside pressure force on the vertical section of the belt balances the horizontal load force on the pivot. Hence, slab retreat resulting from slab pull can be limited by associated thickening of the oceanic asthenosphere. A valve connecting the overpressured inside with the outside world in Figure 6, would allow the fluid to escape down the pressure gradient and the belt would retreat all the way to the right. In nature, slab windows act as such valves and several recent studies have explored slab retreat as a function of the three-dimensional geometry of slabs and slab windows [e.g., *Funiciello et al.*, 2004, 2006; *Piomallo et al.*, 2006; *Stegman et al.*, 2006; *Schellart et al.*, 2007].

[11] We now consider a case in which a load is applied at the lower end and the belt can go freely through the wall on the right (Figure 7). Again, the inside layer thickens and shortens; that is, the trench moves toward right. This time, the force transmitted along the belt is defined by the shear resistance of the fluid as the belt is dragged over it. Also, the continuous motion of the belt will drive fluid into the slab corner on the left and the resulting topographic gradient will cause return flow back to the right. A stage of dynamic equilibrium in Figure 7b is reached when (1) the horizontal pressure force associated with an excess fluid elevation  $\Delta H$  in the slab corner balances the drag force acting on the belt and (2) the pressure gradient associated with a topographic difference between the pivot and the wall  $\Delta H'$  drives return flow toward right balancing the shear flow toward left. We use a shallow-water assumption ( $L \gg H$ ,  $\Delta H$  and  $\Delta H' \ll H$ ) to estimate  $\Delta H$  and  $\Delta H'$ . First, we derive the shear force on the belt through the velocity of the belt. The general equation describing the velocity field in a nonaccreting counterflow cell is

$$u = u_0 \left( 1 - \frac{y}{H} + 3 \left( \frac{y^2}{H^2} - \frac{y}{H} \right) \right), \quad (3)$$

with  $u_0$  being the velocity of the belt [*Turcotte and Schubert*, 1982],  $H$  being the layer thickness, and  $y$  pointing in the vertical direction (Figure 5). The horizontal shear stress  $\tau$  associated with  $u$  is

$$\tau = \frac{\partial u}{\partial y} \mu, \quad (4)$$

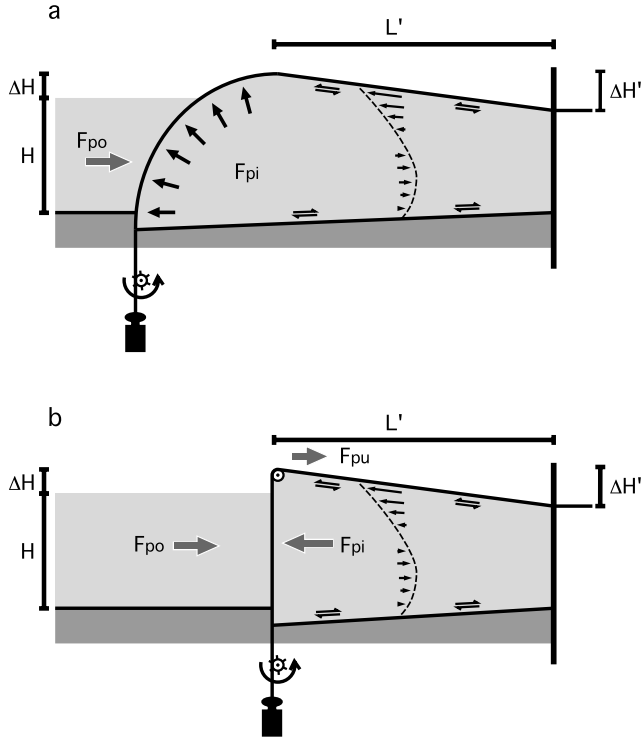


**Figure 7.** The belt in Figure 6 now moves with a constant velocity  $u_0$ . The shear resistance of the fluid defines the force transmitted along the belt.  $F_{pu}$ , shear force on the belt associated with belt motion;  $F_{pi}$  and  $F_{po}$  as in Figure 6. (a) Equilibrium situation is defined by (1) a topographic difference  $\Delta H$  at the trench causing an extra pressure force on the vertical projection of the slab which balances the shear resistance and (2) a total topographic difference along the belt  $\Delta H'$  which drives steady state counterflow. (b) Same case for  $L' \gg H$  and  $H \gg \Delta H$ . If flow-related shear stress is transmitted to the lower surface of the light fluid,  $\Delta H'$  will be larger than  $\Delta H$ . The fluid column at the right side (the “ridge”) that is in equilibrium with a nonmoving slab is less high than the fluid column in the outside world, and the difference depends linearly on plate size and plate velocity (see text for further discussion and equations).

with  $\mu$  being the viscosity of the fluid. Finally, the shear force  $F_{pu}$  pulling on the pivot is simply

$$F_{pu} = L\tau|_{y=0}. \quad (5)$$

[12] Differentiating equation (3) at  $y = 0$  and substituting the result into (4) and (5) yields

$$F_{pu} = -4\mu \frac{u_0 L}{H}, \quad (6)$$

and substituting (6) into (2) leads to

$$\Delta H = 4 \frac{\mu u_0 L}{\rho g H^2}. \quad (7)$$

[13] To determine the total topographic difference along the belt  $\Delta H'$  we use the basic equation for a pressure

gradient driving a counterflow cell without accretion [Turcotte and Schubert, 1982].

$$\frac{dp}{dx} = 6 \frac{\mu u_0}{H^2}. \quad (8)$$

With

$$\frac{dp}{dx} = \frac{\Delta H' \rho g}{L}, \quad (9)$$

it follows that

$$\Delta H' = 6 \frac{\mu u_0 L}{\rho g H^2}, \quad (10)$$

and thus

$$\Delta H' = \frac{3}{2} \Delta H. \quad (11)$$

[14] Hence, a fluid column on the right side of Figure 7 in equilibrium with a stationary slab position is less high than the fluid column in the outside world and the difference ( $\Delta H' - \Delta H$ ) depends linearly on  $L$  (plate size) and  $u_0$  (plate velocity).

[15] A consequence of this result is that two cells like the one in Figure 7 merged at a mutual divergent boundary will not reach a stable geometry if the two cells have different sizes or one belt moves faster than the other (Figure 8). The pressure at the divergent boundary cannot be in equilibrium with two stationary slabs. The smaller (more slowly moving) cell will have a larger equilibrium pressure than the larger (more rapidly moving) one (Figure 8). Any ridge pressure higher than the equilibrium pressure of the smaller (more slowly moving) cell will cause both slabs to advance, i.e., the ocean to expand and the ridge pressure to drop. Any pressure smaller than the equilibrium pressure of the larger (more rapidly moving) cell will cause both cells to shrink and the ridge pressure to rise. For a constant amount of trapped fluid, the ridge pressure will reach a value between the two equilibrium pressures, at which the larger (more rapidly moving) cell would expand at the expense of the smaller (more slowly moving) one (Figure 8). The difference between  $\Delta H$  and  $\Delta H'$  and the associated asymmetry of the model result from the fact that return flow in the channel exerts a shear stress on the lower boundary of the fluid which does not act as a retreat force on the slab. Pressure force associated with the total topographic difference  $\Delta H'$  has to balance the entire shear forces at the bottom and top of the channel whereas pressures force associated with  $\Delta H$  has to balance the shear force on the belt only. Assuming a shear-stress-free lower boundary condition would lead to equal  $\Delta H$  and  $\Delta H'$ .

[16] In a model as in Figure 3, both components of flow, the accretion-related collapse of the oceanic asthenosphere and the plate-motion-related counterflow, cause an asymmetry protecting the larger plate. The larger plate collapses

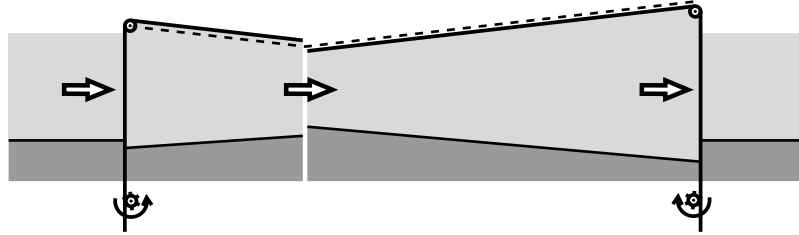


**Figure 8.** Two cells such as in Figure 7 joined at a mutual “ridge.” Solid lines indicate belt positions in equilibrium with nonmoving slabs. If the two cells have different horizontal lengths the system cannot reach a stable configuration. This happens as the height of the fluid column at the ridge which is in equilibrium with a nonmoving slab is not the same for the two cells. A column higher than the equilibrium height of the smaller cell causes both slabs to advance and the fluid level to drop. Conversely, a fluid column at the ridge less high than the equilibrium height of the larger plate causes both slabs to retreat and the fluid level to rise. Any constant fluid level has to be in between the two equilibrium heights (dashed line) and is associated with flow from the smaller cell into the larger one. Hence, the slab of the smaller plate retreats and the slab of the larger one advances.

more slowly than the smaller one as its slab is further away from the pressure minimum at the ridge. Asymmetric counterflow feeds the asthenosphere of the larger plate from the one of the smaller plate.

[17] Figure 9 shows the setup of a very simple one-and-a-half-dimensional finite difference scheme combining these two effects and making a crude prediction of lateral slab motion. The model is discretized in the horizontal direction. Every element tracks volumes of lithosphere and asthenosphere. Lithosphere and asthenosphere have densities of  $3300 \text{ kg/m}^3$  and  $3250 \text{ kg/m}^3$ , respectively. The model is flooded with water (density  $1000 \text{ kg/m}^3$ ) and floats on mesosphere (density  $3260 \text{ kg/m}^3$ ). Plate velocities and ridge location are predefined and can both be asymmetric. The lower boundary of the asthenosphere is fixed in the horizontal direction. Each time step, lithosphere is exchanged between elements according to the local plate velocity and plate thickness. Also, asthenosphere gets accreted into lithosphere according to the relation  $H_L = 2.32\sqrt{kt}$ , with

$H_L$  being the thickness and  $t$  the age of the lithosphere [Turcotte and Schubert, 1982] and  $k$  being  $0.8 \text{ mm}^2/\text{s}$ . Using the above mentioned shallow-water assumption, asthenosphere is exchanged between elements according to plate-motion-related shear flow (Couette flow) and pressure-driven flow (Poiseuille flow). The two element boundaries bordering the oceanic domain are defined as trench boundaries. Lithosphere that moves through these boundaries is simply removed and not added to the adjacent element (Figure 9). The two overriding plate domains consist of  $1000 \text{ km}$  wide arrays of elements without lithosphere and a constant-pressure boundary conditions at the sides of the model. There is no shear flow across the trench boundary. However, there is pressure-driven flow. The pressure gradient across the trench boundary is corrected in the way described in the previous sections. Each step, the shear stress at the plate is integrated from ridge to trench. The resulting force is assumed to be balanced by excess pressure force in the

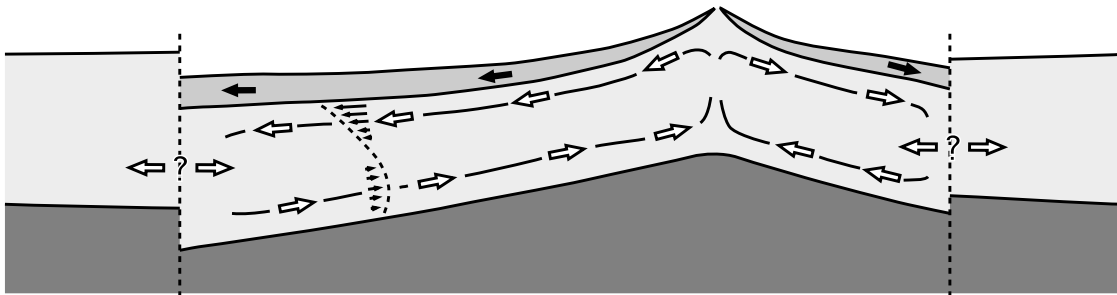


**Figure 9.** Sketch illustrating a simple, 1.5-dimensional, finite difference scheme calculating flow in a model like the one in Figure 3 using a shallow-water approximation. Lower boundary of the asthenosphere is floating with a density contrast of  $10 \text{ kg/m}^3$  toward the substratum. Right and left side have constant pressure boundary conditions. Motion and accretion into lithosphere drive counterflow in the asthenospheric channel. At the trench, the lithosphere is removed. Asthenosphere can flow through the trench into and out of the oceanic domain, but the pressure gradient across the trench is corrected for the shear resistance of the plate; that is, an overpressure on the inside has to balance the shear force dragging at the plate. Flux across the trench is then used to infer slab motion assuming that slabs sail passively in the flow field. See text for more detailed description.

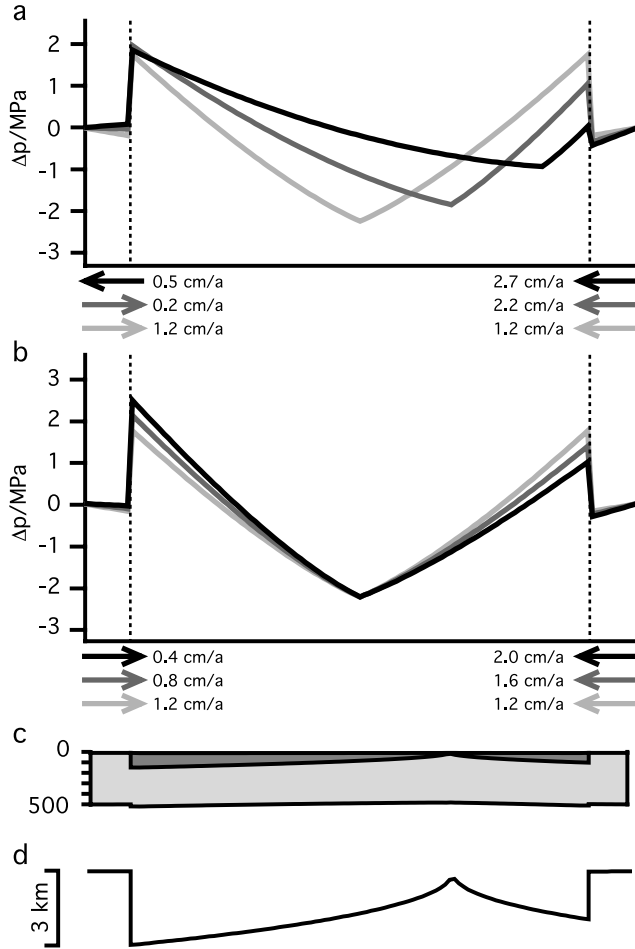


**Figure 10.** Results of model runs. X-axis is a horizontal section across model ocean. Vertical dashed lines indicate trench locations. Figure shows the effect of (a) varying ridge position and (b) ridge motion on the difference between the local pressure in the asthenosphere and the reference pressure at the model boundary. Hence, curves can also be read as predicted dynamic topography across the ocean. Model ocean is 10,000 km wide; the isostatic base of the asthenosphere is at 500 km depth. Ridge positions in Figure 10a are in the middle of the ocean (light gray line), 2000 km away from the middle (gray line), and 4000 km away from the middle (black line). Arrows indicate corresponding predicted lateral slab motions inferred from flux across the trench element. Pressure jumps at the trench illustrate overpressure on the inside balancing the flow-related shear force on the base of the plate. (c) Predicted thickness of lithosphere and asthenosphere for a ridge position 2000 km away from the center. Vertical scale is in kilometers. (d) Predicted water depth for the same model. Differences in dynamic topography are small compared to isostatic differences associated with plate thickening.

asthenosphere from the ocean side on the slab. Thus, the pressure gradient across the trench boundary is calculated using an inside pressure reduced by a pressure difference  $\Delta p$  that would exert a pressure force on the asthenospheric column matching the shear force on the plate. As a result

the inside corner builds up overpressure with respect to the domain of the overriding plate.

[18] As accretion and “subduction” remove material from the oceanic domain, the pressure level drops and the outside asthenosphere flows from the sides into the oceanic domain. We use the steady state flux of asthenosphere across the trench boundaries as an estimate of slab motion. Thus, we assume that slabs drift passively in the mantle flow field.

[19] In a first series of experiments (Figure 10), the model ocean is 10000 km wide, halfspreading rate is 5 cm/a, the isostatic base of the asthenosphere is at 500 km depth, and the viscosity of the mantle is  $10^{19}$  Pas. Figure 10 shows the effects of varying ridge position (Figure 10a) and asymmetric ridge position, i.e., ridge motion (Figure 10b) by means of the pressure in the asthenosphere. For the chosen parameters (a relatively thick asthenosphere with a low viscosity), pressure differences are small. This is also recorded in the modest topography of the base of the asthenosphere (Figure 10c) and in the almost isostatic model topography (Figure 10d). The pressure jump at the trench resulting from the above described pressure correction, illustrates the overpressure of the asthenosphere in the trench corner of the subducting plate. Arrows in Figures 10a and 10b display predicted lateral slab motions inferred from asthenospheric flux across the trench boundary. For a symmetric case (ridge in the center of the ocean/no ridge motion), slab retreat is 1.2 cm/a on both sides of the ocean. Varying the ridge position has a pronounced effect on predicted slab velocities (Figure 10a). For a strongly asym-

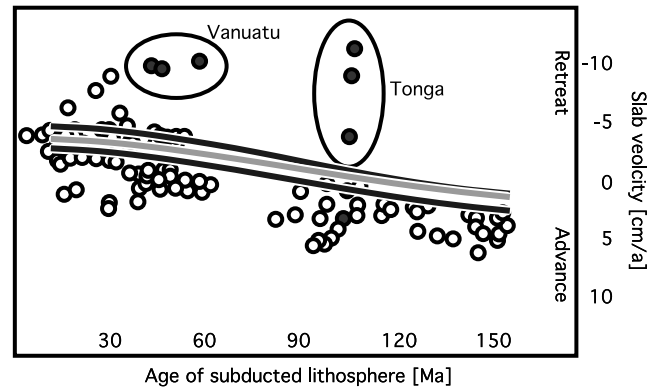


**Figure 11.** Three different model predictions superposed on Figure 2. Model ocean is 12,000 km wide, and halfspreading rate is 7 cm/a. Plate velocities are symmetric. Lines indicate predicted lateral slab velocities for different slab ages. Slab ages are inferred through the distance between ridge and trench. Thus, young ages correspond to small plates, and old ones correspond to large plates. Along a curve, the ridge positions changes. Isostatic base of the asthenosphere is at 500 km depth (light curve) and at 350 km depth (dark curves). The lower black curve is calculated with a distributed influx of  $3.5 \times 10^{-4} \text{ m}^2/\text{s}$  into asthenosphere from the bottom, which reduces the total collapse velocity. Outflux through accretion and subduction is about  $4.8 \times 10^{-4} \text{ m}^2/\text{s}$  for the chosen setup.

metric ridge location (4000 km away from the center), the slab of the larger plate advances with 0.5 cm/a in the direction of the overriding plate whereas the other slab rapidly collapses into the nearby low-pressure zone at the ridge (2.7 cm/a). For asymmetric plate velocities (Figure 10b), the slab of the faster moving plate retreats more slowly than the slab of the slower plate but does not advance for the chosen boundary conditions. The total collapse rate of the ocean (the sum of the two retreat velocities) is nearly the same for all experiments, since it has to match the outflux of material from the oceanic domain. This outflux is determined by the thicknesses and velocities of the plates, hence, by the boundary conditions. Only for very asymmetric ridge positions, the nonlinear growth rate of the plates leads to a noticeable reduction of the total outflux compared to a symmetric situation and the predicted total collapse velocity is slightly smaller (Figure 10a).

[20] For a fixed total ocean size, the above model predicts retreat velocities of slabs decreasing with increasing distance from the ridge. This distance corresponds to the age of the subducted lithosphere. The model thus offers an explanation for the observed negative correlation between retreat velocity and slab age in the Pacific. Figure 11 superposes predictions of three different models on top of the Pacific data of *Heuret and Lallemand* [2005]. Model dimensions are slightly different from the previous model and more “Pacific.” The width of the ocean is 12000 km and half-spreading rate is 7 cm/a. Plate velocities, however, are symmetric. The light gray curve is calculated using a 500 km deep isostatic base of the asthenosphere, the two black ones using a 350 km deep base. The model represented by the lower black line has a distributed influx of asthenosphere from the lower boundary which partly compensates the accretion into the lithosphere. Lines indicate calculated retreat velocities for a certain lithospheric age. Hence, the ridge position varies along a curve. Each point on a curve has a corresponding point, which represents the paired trench on the other side of the same ocean. With a 12000 km wide ocean and a half-spreading rate of 7 cm/a, the ages of the two subducting plates sum up to about 170 Ma. Obviously, the predictions of these simple models are only very crude fits. They are meant to show that the model can explain the data trend and that predicted variations of trench velocities have about the right magnitude. The thickness of the asthenospheric layer and an influx into the asthenosphere from below can be used to improve the fit (black curves in Figure 11). The range of calculated trench velocities increases with decreasing thickness of the asthenospheric layer. Hence, decreasing the thickness promotes the asymmetry of the model, i.e., the slope of the curve in Figure 11. Also, a curve can be shifted up and down by introducing a flux into the asthenospheric reservoir from below, since refilling the asthenosphere allows to control the total collapse velocity. Calculations in Figure 11 neglect ridge motion. The higher velocity of the larger plate in the Pacific increases the asymmetry of the east and west side. Using the setup of Figure 11 with the ridge located 3000 km away from one trench and a ridge velocity of 4 cm/a in the direction of the

larger plate, yields a retreat velocity of 3.8 cm/a on the side of the smaller plate and an advance velocity of 1.22 cm/a on the larger side.

### 3. Discussion

[21] We propose that the overall picture of trench motions in the Pacific is governed by the asymmetric large-scale plate configuration. Recent models attribute absolute trench motion to the local framework of a subduction zone, mostly to properties of the slab, such as width, depth, or age. Also, the upper plate motion away from the trench has been used to explain advancing slabs on the eastern side of the Philippine sea plate [*Scholz and Campos*, 1995]. The fundamental difference of our model compared to previous ones is the assumption that slabs are rooted in the mantle. In our concept, absolute motions of slabs image the flow pattern of asthenosphere rather than the capacity of a slab to plow through it. Several studies identified mantle flow around particular narrow slabs [e.g., *Abratis and Worner*, 2001; *Faccenna et al.*, 2001]. However, *Dvorkin et al.* [1993] already showed that the resistance of the asthenosphere to a plowing slab is very sensitive to slab width and proposed that wide slabs should be about stationary in the local mantle frame. Some recent physical and numerical modeling studies investigate the relationship between slab width and retreat velocity [*Bellahsen et al.*, 2005; *Royden and Husson*, 2006; *Funiciello et al.*, 2006; *Stegman et al.*, 2006; *Schellart et al.*, 2007]. These models use resisting boundaries at the bottom of the asthenospheric layer and investigate trench retreat accommodated by horizontal flow of asthenosphere around the slab. The results generally confirm that increasing the slab width decreases retreat velocity but do not suggest negligible velocities for slabs even wider than 1000 km. However, most studies assume enormously wide slab windows, often as wide as the slab itself, allowing for very large wavelength flow around the slab. Wide slabs surrounding the Pacific do not have windows of that dimension, except for two outstanding examples. The Tonga slab ends toward north and the Vanuatu slab toward southeast creating huge gaps in the slab curtain north and south of the mutual back arc, the Fiji sea [*Chen and Brudzinski*, 2001; *Pelletier et al.*, 1998]. These two slabs represent the most prominent outliers in Figure 2 [*Heuret and Lallemand*, 2005] in retreating much faster than would be predicted by the overall data trend. Both slabs, especially the Tonga slab, show a pronounced increase of retreat velocity toward the slab end (Figure 1) [*Heuret and Lallemand*, 2005; *Schellart et al.*, 2007].

[22] Among the strongest arguments for horizontal counterflow in the asthenosphere is the existence of the abyssal planes, i.e., the deviation of the ocean floor topography from the isostatic depth-age curve [*Morgan and Smith*, 1992]. The model of asymmetric flow presented here predicts asymmetric topography on the two flanks of the diverging plate boundary. Plots of pressure variations in Figures 10a and 10b can be viewed as variations in dynamic topography. For an asymmetric ridge position, the steeper pressure gradient on the shorter ridge flank should lead to

this flank being shallower (Figure 10a). This is indeed observed in the Pacific. The eastern slope of the Pacific rise is on average shallower than the western side [Doglioni *et al.*, 2003]. This is especially the case where the ridge is close to the continent, that is where the plate configuration is extremely asymmetric. As mentioned above, the total amplitude of dynamic topography is small for the chosen setup and in the order of a hundred meters. This is far less than what is desired to explain the flat abyssal plains [Morgan and Smith, 1992] (Figure 10d). Also the predicted asymmetry of the ridge is less pronounced than the observed one. However, the amplitude of dynamic topography scales linearly with

the viscosity of the asthenosphere and is extremely sensitive to asthenospheric thickness variations. The used thickness of 500 km is rather large. Using a thinner asthenosphere that is partly refilled would improve both the predicted asymmetry of trench motions and the predicted topography of the ocean (Figures 10 and 11).

[23] **Acknowledgments.** We thank Thorsten Becker, Onno Oncken and an anonymous reviewer for thorough comments. Claudio Faccenna provided comments on an earlier version of this manuscript.

## References

- Abratis, M., and G. Worner (2001), Ridge collision, slab-window formation, and the flux of Pacific asthenosphere into the Caribbean realm, *Geology*, *29*, 127–130, doi:10.1130/0091-7613(2001)029<0127:RCSWFA>2.0.CO;2.
- Becker, T. W. (2006), On the effect of temperature and strain-rate dependent viscosity on global mantle flow, net rotation, and driving forces, *Geophys. J. Int.*, *167*, 943–957, doi:10.1111/j.1365-246X.2006.03172.x.
- Bellahsen, N., C. Faccenna, and F. Fucicello (2005), Dynamics of subduction and plate motion in laboratory experiments: Insights into the “plate tectonics” behavior of the Earth, *J. Geophys. Res.*, *110*, B01401, doi:10.1029/2004JB002999.
- Bird, P. (2003), An updated digital model of plate boundaries, *Geochem. Geophys. Geosyst.*, *4*(3), 1027, doi:10.1029/2001GC000252.
- Chase, C. G. (1978), Extension behind island arcs and motion relative to hot spots, *J. Geophys. Res.*, *83*, 5385–5387, doi:10.1029/JB083iB11p05385.
- Chase, C. G. (1979), Asthenospheric counterflow: A kinematic model, *Geophys. J. R. Astron. Soc.*, *56*, 1–18.
- Chen, W.-P., and M. R. Brudzinski (2001), Evidence for a large-scale remnant of subducted lithosphere beneath Fiji, *Science*, *292*, 2475–2479, doi:10.1126/science.292.5526.2475.
- DeMets, C., R. G. Gordon, D. F. Argus, and S. Stein (1994), Effect of recent revisions to the geomagnetic reversal time scale on estimates of current plate motion, *Geophys. Res. Lett.*, *21*, 2191–2194, doi:10.1029/94GL02118.
- Doglioni, C., E. Carminati, and E. Bonatti (2003), Rift asymmetry and continental uplift, *Tectonics*, *22*(3), 1024, doi:10.1029/2002TC001459.
- Dvorkin, J., A. Nur, G. Mavko, and Z. Ben-Avraham (1993), Narrow subducting slabs and the origin of back-arc basins, *Tectonophysics*, *227*, 63–79, doi:10.1016/0040-1951(93)90087-Z.
- Enns, A., T. W. Becker, and H. Schmeling (2005), The dynamics of subduction and trench migration for viscosity stratification, *Geophys. J. Int.*, *160*, 761–775, doi:10.1111/j.1365-246X.2005.02519.x.
- Faccenna, C., F. Fucicello, D. Giardini, and P. Lucente (2001), Episodic back-arc extension during restricted mantle convection in the central Mediterranean, *Earth Planet. Sci. Lett.*, *187*, 105–116, doi:10.1016/S0012-821X(01)00280-1.
- Faccenna, C., P. Piromallo, A. Crespo-Blanc, L. Jolivet, and F. Rossetti (2004), Lateral slab deformation and the origin of the western Mediterranean arcs, *Tectonics*, *23*, TC1012, doi:10.1029/2002TC001488.
- Faccenna, C., A. Heuret, F. Fucicello, S. Lallemand, and T. W. Becker (2007), Predicting trench and plate motion from the dynamics of a strong slab, *Earth Planet. Sci. Lett.*, *257*, 29–36, doi:10.1016/j.epsl.2007.02.016.
- Forsyth, D. W., and S. Uyeda (1975), On the relative importance of the driving forces of plate motion, *Geophys. J. R. Astron. Soc.*, *43*, 163–200.
- Fucicello, F., C. Faccenna, and D. Giardini (2004), Role of lateral mantle flow in the evolution of subduction systems: Insights from laboratory experiments, *Geophys. J. Int.*, *157*, 1393–1406, doi:10.1111/j.1365-246X.2004.02313.x.
- Fucicello, F., M. Moroni, C. Piromallo, C. Faccenna, A. Cenedese, and H. A. Bui (2006), Mapping mantle flow during retreating subduction: Laboratory models analyzed by feature tracking, *J. Geophys. Res.*, *111*, B03402, doi:10.1029/2005JB003792.
- Gautier, P., J. P. Brun, R. Moriceau, D. Sokoutis, J. Martinod, and L. Jolivet (1999), Timing, kinematics and cause of Aegean extension: A scenario based on a comparison with simple analogue experiments, *Tectonophysics*, *315*, 31–72, doi:10.1016/S0040-1951(99)00281-4.
- Gripp, A. E., and R. G. Gordon (2002), Young tracks of hotspots and current plate velocities, *Geophys. J. Int.*, *150*, 321–361, doi:10.1046/j.1365-246X.2002.01627.x.
- Gurnis, M., C. Hall, and L. Lavier (2004), Evolving force balance during incipient subduction, *Geochem. Geophys. Geosyst.*, *5*, Q07001, doi:10.1029/2003GC000681.
- Heuret, A., and S. Lallemand (2005), Plate motions, slab dynamics and back-arc deformation, *Phys. Earth Planet. Inter.*, *149*, 31–51, doi:10.1016/j.pepi.2004.08.022.
- Lallemand, S., A. Heuret, and D. Boutelier (2005), On the relationships between slab dip, back-arc stress, upper plate absolute motion, and crustal nature in subduction zones, *Geochem. Geophys. Geosyst.*, *6*, Q09006, doi:10.1029/2005GC000917.
- Malinverno, A., and W. B. F. Ryan (1986), Extension in the Tyrrhenian sea and shortening in the Apennines as result of arc migration driven by sinking of the lithosphere, *Tectonics*, *5*, 227–245, doi:10.1029/TC005i002p00227.
- Moberly, R. (1972), Origin of lithosphere behind island arcs with reference to the western Pacific, *Mem. Geol. Soc. Am.*, *132*, 32–55.
- Molnar, P., and T. Atwater (1978), Interarc spreading and cordilleran tectonics as alternates related to the age of subducted oceanic lithosphere, *Earth Planet. Sci. Lett.*, *41*, 330–340, doi:10.1016/0012-821X(78)90187-5.
- Morgan, J. P., and W. H. F. Smith (1992), Flattening of the seafloor depth-age curve as a response to asthenospheric flow, *Nature*, *359*, 524–527, doi:10.1038/359524a0.
- Morgan, J. P., W. J. Morgan, Y.-S. Zhang, and W. H. F. Smith (1995), Observational hints for a plume-fed, suboceanic asthenosphere and its role in mantle convection, *J. Geophys. Res.*, *100*, 12,753–12,767, doi:10.1029/95JB00041.
- Morgan, W. J. (1971), Convection plumes in the lower mantle, *Nature*, *230*, 42–43, doi:10.1038/230042a0.
- Parmentier, E. M., and J. E. Oliver (1979), A study of shallow mantle flow due to the accretion and subduction of lithospheric plates, *Geophys. J. R. Astron. Soc.*, *57*, 1–22.
- Pelletier, B., S. Calmant, and R. Pillet (1998), Current tectonics of the Tonga-New Hebrides Region, *Earth Planet. Sci. Lett.*, *164*, 263–276, doi:10.1016/S0012-821X(98)00212-X.
- Piromallo, C., T. W. Becker, F. Fucicello, and C. Faccenna (2006), Three-dimensional instantaneous mantle flow induced by subduction, *Geophys. Res. Lett.*, *33*, L08304, doi:10.1029/2005GL025390.
- Pysklywec, R. N., and M. Ishii (2005), Time dependent subduction dynamics driven by the instability of stagnant slabs in the transition zone, *Phys. Earth Planet. Inter.*, *149*, 115–132, doi:10.1016/j.pepi.2004.08.019.
- Richards, M. A., W. S. Yang, J. R. Baumgardner, and H. P. Bunge (2001), Role of a low-viscosity zone in stabilizing plate tectonics: Implications for comparative terrestrial planetology, *Geochem. Geophys. Geosyst.*, *2*, doi:10.1029/2000GC000115.
- Rizzetto, C., A. M. Marotta, and R. Sabadini (2004), The role of trench retreat on the geometry and stress regime in the subduction complexes of the Mediterranean, *Geophys. Res. Lett.*, *31*, L11604, doi:10.1029/2004GL019889.
- Royden, L. H., and L. Husson (2006), Trench motion, slab geometry and viscous stresses in subduction zones, *Geophys. J. Int.*, *167*, 881–905, doi:10.1111/j.1365-246X.2006.03079.x.
- Schellart, W. P., J. Freeman, D. R. Stegman, L. Moresi, and D. May (2007), Evolution and diversity of subduction zones controlled by slab width, *Nature*, *446*, 308–311, doi:10.1038/nature05615.
- Scholz, C. H., and J. Campos (1995), On the mechanism of seismic decoupling and back arc spreading at subduction zones, *J. Geophys. Res.*, *100*, 22,103–22,116, doi:10.1029/95JB01869.
- Schubert, G., and D. L. Turcotte (1972), One-dimensional model of shallow mantle convection, *J. Geophys. Res.*, *77*, 945–951, doi:10.1029/JB077i005p00945.
- Schubert, G., C. Froidevaux, and D. Yuen (1976), Oceanic lithosphere and asthenosphere: Thermal and mechanical structure, *J. Geophys. Res.*, *81*, 3525–3540, doi:10.1029/JB081i020p03525.
- Small, C., and L. V. Danyushevsky (2003), Plate-kinematic explanation for mid oceanic-ridge depth discontinuities, *Geology*, *31*, 399–402, doi:10.1130/0091-7613(2003)031<0399:PEFMDD>2.0.CO;2.
- Stegman, D. R., J. Freeman, W. P. Schellart, L. Moresi, and D. May (2006), Influence of trench width on subduction retreat in 3-D models of slab rollback, *Geochem. Geophys. Geosyst.*, *7*, Q03012, doi:10.1029/2005GC001056.
- Steinberger, B., R. Sutherland, and R. J. O’Connell (2004), Prediction of Emperor-Hawaii seamount

- locations from a revised model of global motion and mantle flow, *Nature*, 430, 167–173, doi:10.1038/nature02660.
- Turcotte, D. L., and G. Schubert (1982), *Geodynamics—Application of Continuum Physics to Geological Problems*, 450 pp., John Wiley, Hoboken, N. J.
- Uyeda, S., and H. Kanamori (1979), Back-arc opening and the mode of subduction, *J. Geophys. Res.*, 84, 1049–1061, doi:10.1029/JB084iB03p01049.
- University, 61 Route 9W, Palisades, NY 10964-8000, USA.
- T. J. Nagel, Steinmann Institut, Universität Bonn, Nussallee 8, D-53115 Bonn, Germany. (tnagel@uni-bonn.de)
- W. R. Buck, A. Malinverno, and W. B. F. Ryan, Lamont-Doherty Earth Observatory of Columbia